

Electronic Supplementary Material (ESI) for Journal of Materials Chemistry A
This journal is © The Royal Society of Chemistry 2018

Electronic Supplementary Material

High-performance Lithium-Organic Batteries by Achieving 16-Lithium Storage in Poly(imine-anthraquinone)

Zengming Man,^a Peng Li,^a Dong Zhou,^{*b} Rui Zang,^a Shijian Wang,^b Pengxin Li,^a Shuaishuai Liu,^a Xuemei Li,^a Yuhan Wu,^a Xiaohui Liang^a and Guoxiu Wang^{*b}

^a College of Material Science and Engineering, Nanjing University of Aeronautics and Astronautics, Nanjing, 210016, P. R. China

^b Centre of Clean Energy Technology, Faculty of Science, University of Technology, Sydney, NSW 2007, Australia

* Corresponding to: dong.zhou@uts.edu.au, guoxiu.wang@uts.edu.au

Computational Method.

(1) Capacity contribution of pure PIAQ

The composite capacity of pure PIAQ can be regarded as the contribution of two components, as described by the following equation:

$$C_{PIAQ} = C_{p-PIAQ} * P_{p-PIAQ} + C_{KB} * P_{KB} \quad \text{Eq S1}$$

where C_{p-PIAQ} , C_{PIAQ} , C_{KB} represent the capacities of pure PIAQ, PIAQ electrode material and ketjen black, respectively. P_{PIAQ} and P_{KB} correspond to the mass percent of PIAQ and ketjen black in the PIAQ electrode material composite.

$$C_{p-PIAQ} = (1097 - 499 * \frac{2}{9}) / \frac{7}{9} = 1268 \text{ mA h g}^{-1} \quad \text{Eq S2}$$

(2) DFT simulation.

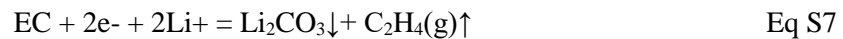
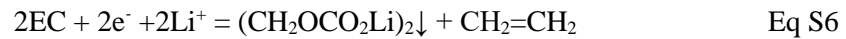
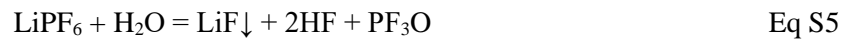
The theoretical calculations were based on the DFT in conjunction with the projector-augmented-wave (PAW) potential in the CASTEP module of MS. The binding energy is defined as the following equation:

$$E_b(\text{Li}) = (E_{PIAQ+ n * E_{Li}} - E_{Li-PIAQ}) / n \quad \text{Eq S3}$$

where n is the number of lithium atoms attached to the pristine PIAQ, and E_{Li} , E_{PIAQ} , and $E_{Li-PIAQ}$ are the corresponding energies of the isolated lithium atom, the pristine PIAQ, and Li-inserted PIAQ, respectively. The Gibbs free energy (ΔG) was applied to explore and determine the most stable Li-inserted state, which is defined as the following equation:

$$\Delta G = E_{Li-PIAQ} - E_{PIAQ}. \quad \text{Eq S4}$$

Equation to explain the compositions of SEI film.



Electronic Supplementary Figures and Tables

Table S1. Element analysis of the PIAQ

	C	H	O	N
Theoretical (wt%)	78.58	3.57	9.52	8.33
Estimated (wt%)	78.61	3.48	9.54	8.37

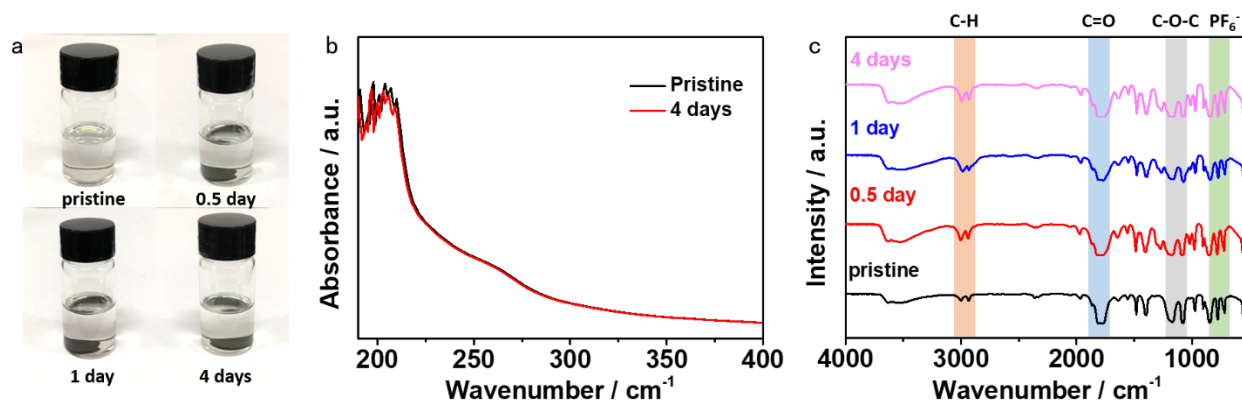


Figure S1. Photographs of the pristine 1.0 M LiPF₆ in EC/DEC (volume ratio=1:1) electrolyte and the 10 wt% PIAQ powder-containing electrolytes after different stirring time. The corresponding b) UV-vis and c) FTIR spectra of the pristine electrolyte and the filtrate of PIAQ powder-containing electrolytes after different stirring time.

To identify the solubility of PIAQ in the organic electrolyte, 10 wt% PIAQ was stirred in 1.0 M LiPF₆ in EC/DEC (volume ratio=1:1) liquid electrolyte. As seen from Figure S1a, the colour of electrolyte almost unchanged after stirring for 4 days, which is consistent with the nearly invariable UV-vis spectra (Figure S1b). Furthermore, no characteristic peaks related to PIAQ appears in the FTIR of the filtered PIAQ-containing electrolyte after stirring for 4 days (Figure S1b; 2997 and 2930 cm⁻¹: -C-H stretching from the methylene group of EC and DEC; 1815 and 1785 cm⁻¹: C=O stretching; 1176 and 1067 cm⁻¹: -C-O-C stretching; 870-830 cm⁻¹: PF₆⁻ from LiPF₆).^[1] This clearly indicates a negligible solubility of PIAQ in organic electrolytes.

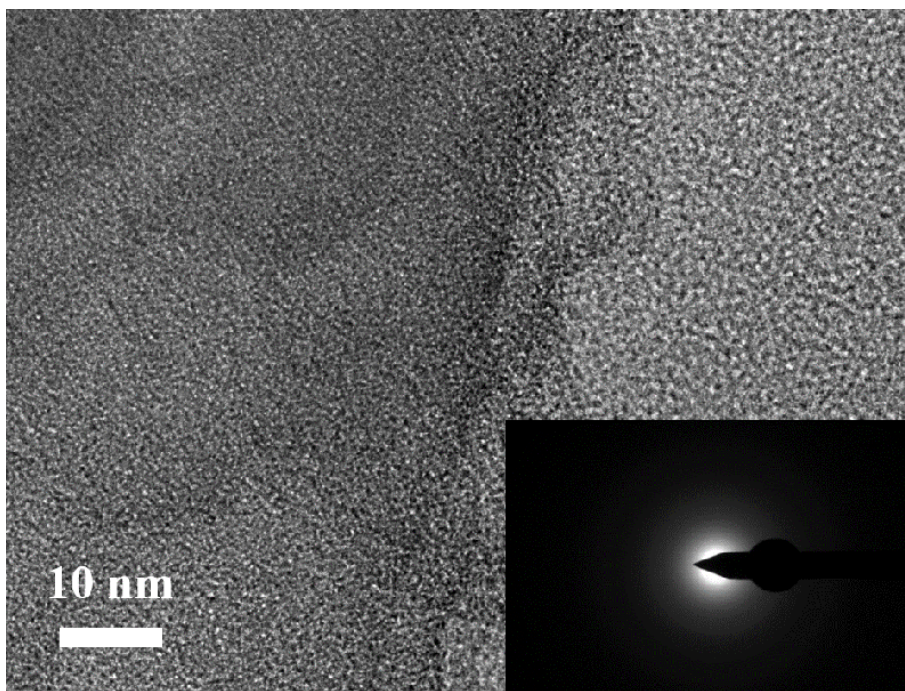


Figure S2. HRTEM and selected area electron diffraction (SAED, insert) images of PIAQ.

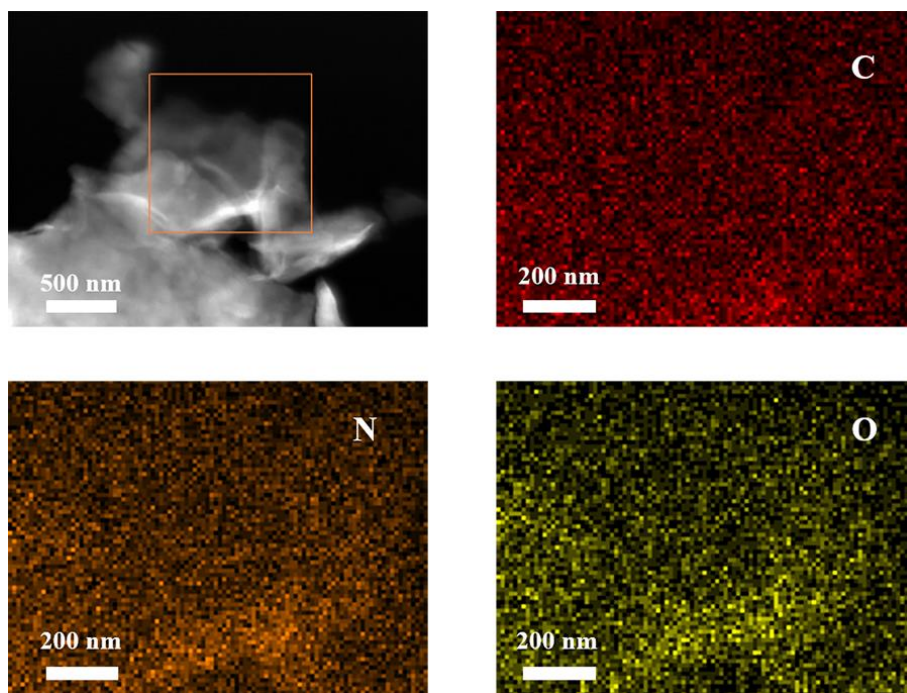


Figure S3. EDS mappings of PIAQ.

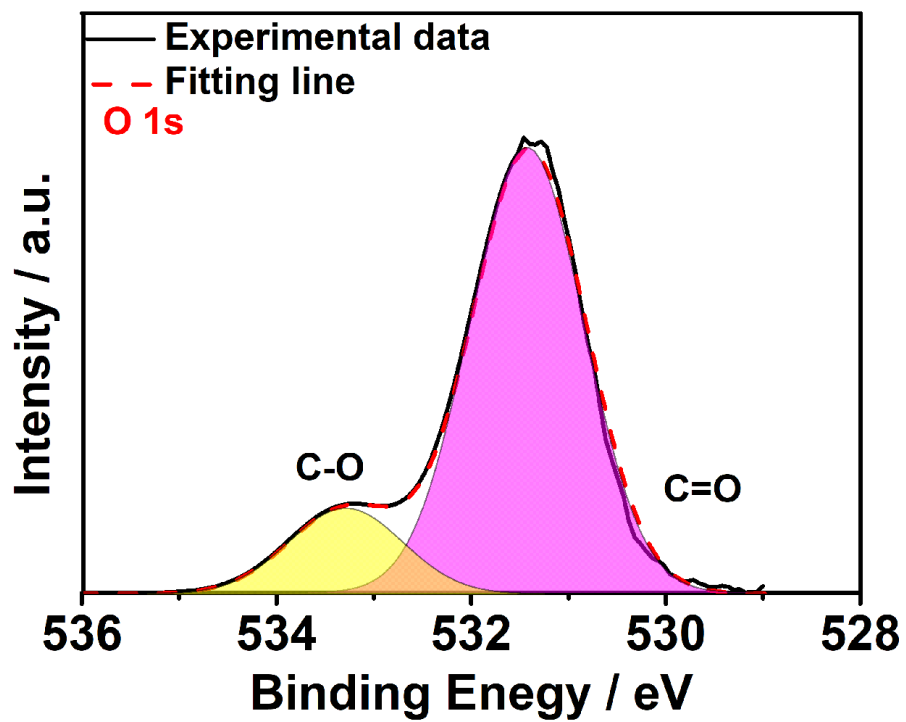


Figure S4. O 1s XPS spectra of PIAQ.

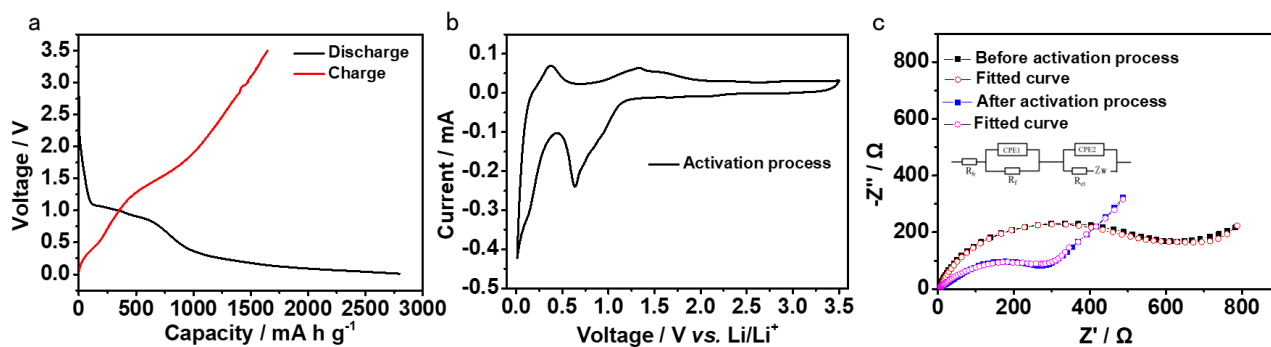


Figure S5. The activation process of the Li/PIAQ cell. a) The galvanostatic discharge/charge profiles at 100 mA g^{-1} in the voltage range $0.01\text{-}3.5 \text{ V vs. Li/Li}^+$; b) The corresponding CV curves at a scan rate of 0.1 mV s^{-1} ; c) experimental and simulation EIS curves of the PIAQ cell before and after activation process.

An irreversible electrochemical reduction current peak appears at 0.6 V during the activation process, which corresponds to the electrolyte decomposition and the formation of a solid electrolyte interfacial (SEI) film on the electrode surface and other by-reactions. ^[2,3]

As can be seen from **Figure S5**, the experimental and simulated spectra are quite well matched. According to the equivalent circuit, the intersection of the diagram with the real axis refers to a bulk resistance (R_b), reflecting the resistance of electrodes and electrolyte/separator. The depressed semicircle at high frequency can be attributed to the solid electrolyte interface resistance (R_f) and $CPE1$, while the depressed semicircle at medium frequency can be ascribed to the charge transfer resistance (R_{ct}) and $CPE2$. Instead of the capacitance of the passivation layer (C_f) and double-layer capacitance (C_{dl}), $CPE1$ and $CPE2$ are the constant phase elements used to take the roughness of the particle surface into account. The line at low frequency is equivalent to the Warburg impedance (Z_w), which is related to the sodium ion diffusion within the particles. ^[4]

Table S2. EIS simulation results of the changes in interface resistance (R_f and R_{ct}) before and after electrode activation process.

Battery sample	Before activation process		After activation process	
	R_f (Ω)	R_{ct} (Ω)	R_f (Ω)	R_{ct} (Ω)
PIAQ	527.1	346.1	360.0	53.5

It is seen that the interfacial resistance (R_f) of the PIAQ electrode decreases from 527.1 Ω to 360.0 Ω after the activation process, which is mainly due to the construction of a stable solid electrolyte interface (SEI) against the Li^+ -consuming side reactions with electrolytes.^[5] Meanwhile, the charge-transfer resistance (R_{ct}) significantly decreases from 346.1 Ω to 53.5 Ω , which can be attributed to the enhanced diffusion kinetics of Li^+ insertion/extraction.^[6] Such decreased R_f and R_{ct} result in a reduced polarization, which benefits an excellent battery performance in the subsequent cycling.

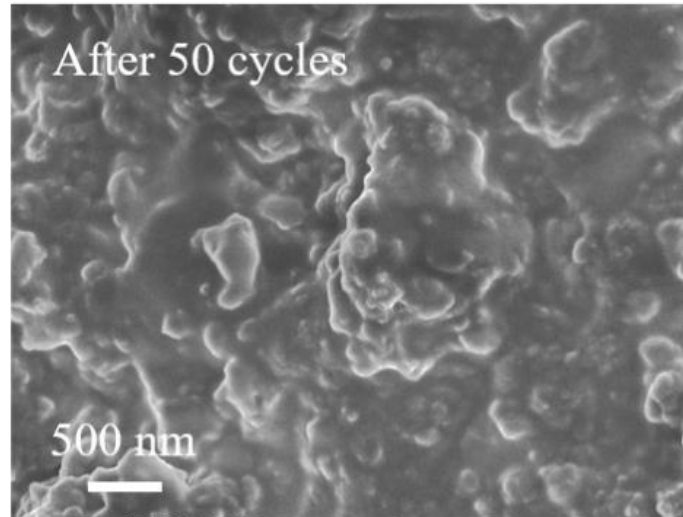


Figure S6. SEM image of the PIAQ electrode after 50 cycles.

It can be seen from Figure S6 that the surface of PIAQ electrode remained integrity without defects such as cracks or holes after 50 cycles, indicating the structural robustness of the PIAQ material. Furthermore, compared with the electrode surface after 15 cycles, the electrode surface after 50 cycles became smoother, mainly due to the accumulated solid electrolyte interface (SEI) film during the cycling.

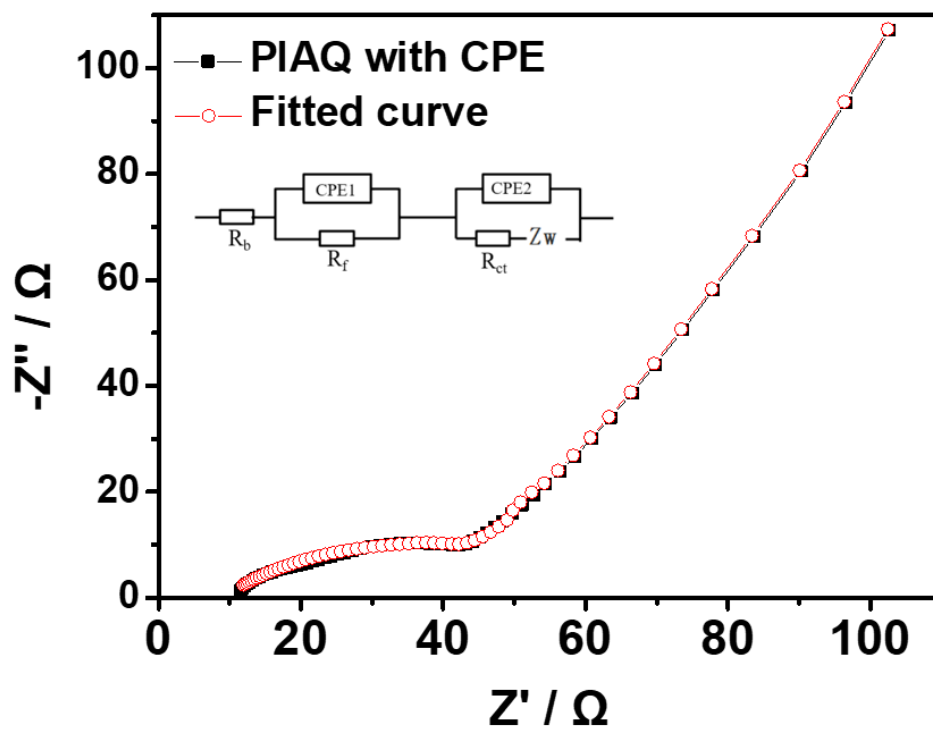


Figure S7. Experimental and simulation EIS curves of the PIAQ cell using an equivalent circuit shown in inset.

Table S3. EIS simulation results from **Figure S7**.

Battery sample	After 1st cycle			After 100th cycle		
	$R_b (\Omega)$	$R_f (\Omega)$	$R_{ct} (\Omega)$	$R_b (\Omega)$	$R_f (\Omega)$	$R_{ct} (\Omega)$
PIAQ	7.5	26.2	50.5	9.2	186.4	45.1

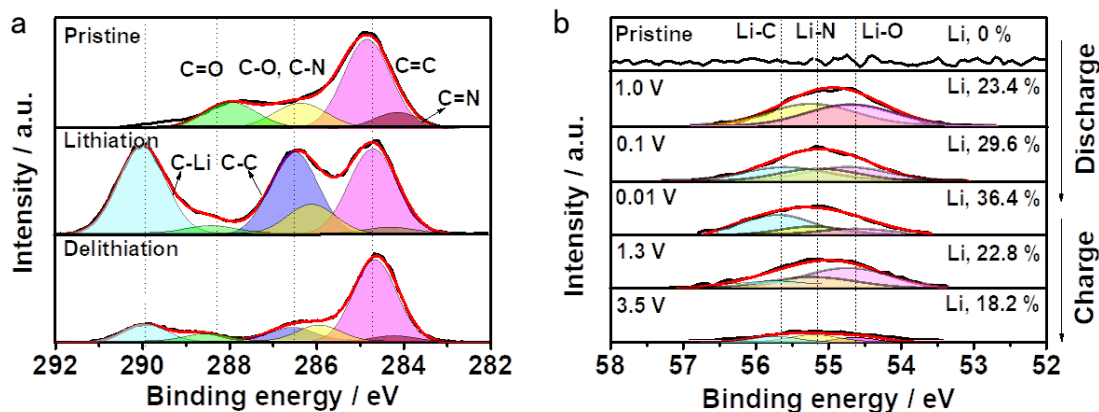


Figure S8 XPS spectra for PIAQ electrode. a) C 1s scan of the pristine PIAQ electrode and PIAQ electrodes after lithiation and delithiation process, b) Li 1s XPS spectra of the PIAQ electrode under different states.

X-ray photoelectron spectroscopy (XPS) of the PIAQ electrode was measured to further probe the Li-storage mechanism. As shown in Figure S8a, peaks at around 288.5, 286.5, 284.8, and 284.3 eV appear in the pristine PIAQ electrode, corresponding to C=O, C-O and C-N, C=C, and C=N groups, respectively. After the lithiation (discharge) process, the intensities of C=N, C=C and C=O peaks decrease; While a C-Li peak at 289.9 eV appear and the intensity obviously increases.^[7] After the lithiation (discharge) process, the intensities of C=N, C=C and C=O peaks reduce, while the intensity C-Li peak obviously increases. This corresponds to the lithiation reaction at the C=N, C=O, and aromatic C=C groups on benzene rings in the PIAQ anode. Furthermore, the area ratio of the C-C peak to C=C peak increases after the lithiation process, and then drops to the original level after the following delithiation process. This demonstrates the reversible transformation between C=C and C-C groups on benzene rings in the PIAQ structure, further confirming the participation of benzene rings in the lithium storage process of PIAQ.

Figure S8b shows the Li 1s spectra of PIAQ electrode under different voltage states. The XPS spectra of the Li1s signal for the PIAQ electrode under different charge/discharge states could be fitted into three sub-peaks, which indicates that Li ions are inserted into the PIAQ electrode at three different sites. When the voltage is discharged to 1.0 V, the peaks appearing at 55.1 and 54.6 eV can be ascribed to the formation of Li-N and Li-O bonds originating from reduction of Schiff base structure and quinone structure. When the voltage is discharged to 0.1 V, a new peak at 55.6 eV can be assigned to the Li-C bond originating from the Li⁺ inserted into benzene ring,^[8] which is consistent with the CV curves in Figure 3a. After the PIAQ is fully discharged to 0.01V, the peak of Li-C bond reached the maximum value, indicating a large amount of Li⁺ have inserted into aromatic benzene rings. The content of Li⁺ fully insertion is calculated as ~36.4 % according to the XPS result, which is well consistent with the theory value when 16 Li⁺ inserted into PIAQ electrode (34.3 %). The peak intensity of Li-C decreases and the peak intensities of Li-N and Li-O increase during the following charging processes, demonstrating an excellent electrochemical reversibility of the PIAQ electrode.

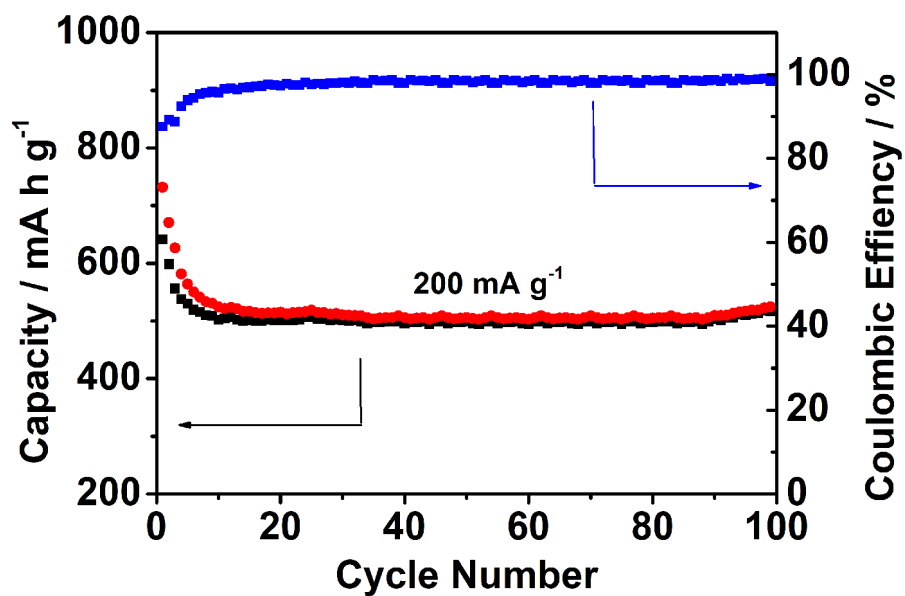
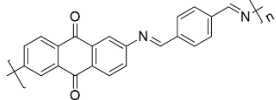
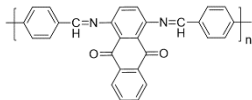
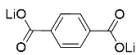
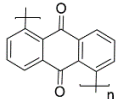
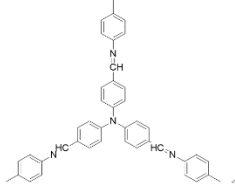


Figure S9. Charge/discharge curves of a cell with a cathode made of 90 wt% Ketjen black, and 10 wt% CMC binder. 1.0 M LiPF₆ dissolved in EC/DEC (volume ratio=1:1) electrolyte, and Li foil as anode. The capacity of Ketjen black was stable at 499 mA h g⁻¹ at 200 mA g⁻¹.

Table S4. Comparison diagram of the electrochemical performance of PIAQ with other organic anode materials reported before.

Material	Structure	Practical Capacity (mA h g ⁻¹)/ Current density (mA g ⁻¹)	Capacity retention (mA h g ⁻¹)/ cycle number/ Current density (mA g ⁻¹)	Reference
1		1413/200	1097/100/200	This work
	PIAQ	1163.5/1000	486/1000/1000	
2		175/10	157/100/10	[9]
	PSB			
3		300/42.2	234/50/42.2	[10]
	Li₂C₈H₄O₄			
4		220/52	148/100/52	[11]
	P15AQ			
5	Humic acid	484/20	180/200/40	[12]
6		140/100	127/400/268	[13]
	Hyperbranched PSB			

Reference

- [1] L. D. Ellis, S. Buteau, S. G. Hames, L. M. Thompson, D. S. Hall, and J. R. Dahn, *J. Electrochem. Soc.*, 2018, **165**, A256-A262.
- [2] J. Liang, X. Y. Yu, H. Zhou, H. B. Wu, S. J. Ding and X. W. Lou, *Angew. Chem. Int. Ed.*, 2014, **53**, 12803-12807.
- [3] X. S. Zhou, L. J. Wan and Y. G. Guo, *Adv. Mater.*, 2013, **25**, 2152-2157.
- [4] D. Zhou, Y. Chen, B. H. Li, H. B. Fan, F. L. Cheng, D. Shanmukaraj, T. Rojo, M. Armand and G. X. Wang, *Angew. Chem. Int. Ed.*, 2018, **57**, 10168-10172.
- [5] J. Alvarado, M. A. Schroeder, M. H. Zhang, O. Borodin, E. Gobrogge, M. Olguin, M. S. Ding, M. Gobet, S. Greenbaum, Y. S. Meng and K. Xu, *Mater. Today*, 2018, **21**, 341-353.
- [6] Y. M. Sun, X. L. Hu, W. Luo, F. F. Xia, and Y. H. Huang, *Adv. Funct. Mater.*, 2013, **23**, 2436-2444.
- [7] Z. Lei, Q. Yang, Y. Xu, S. Guo, W. Sun, H. Liu, L. P. Lv, Y. Zhang and Y. Wang, *Nat. Commun.*, 2018, **9**, 576.
- [8] H. J. Ye, F. Q. Jiang, H. Q. Li, Z. Xu, J. Yin and H. Zhu, *Electrochim. Acta.*, 2017, **253**, 319-323.
- [9] [2] X. F. Feng, W. Zhao, H. X. Ju, L. Zhang, Y. F. Ye, W. H. Zhang, J. F. Zhu, *Org. Electron.*, 2012, **13**, 1060-1067.
- [10] M. Armand, S. Grugeon, H. Vezin, S. Laruelle, P. Ribiere, P. Poizot and J. M. Tarascon, *Nat. Mater.*, 2009, **8**, 120-125.
- [11] Z. P. Song, Y. M. Qian, M. L. Gordin, D. H. Tang, T. Xu, M. Otani, H. Zhan, H. S. Zhou and D. H. Wang, *Angew. Chem. Int. Ed.*, 2015, **54**, 13947-13951.
- [12] H. Zhu, J. Yin, X. Zhao, C. Wang and X. Yang, *Chem. Commun.*, 2015, **51**, 14708-14711.
- [13] Y. Sun, Y. Sun, Q. Pan, G. Li, B. Han, D. Zeng, Y. Zhang and H. Cheng, *Chem. Commun.*, 2016, **52**, 3000-3002.